Slow-Light Enhanced Liquid and Gas Sensing Using 2-D Photonic Crystal Line Waveguides—A Review

Anuj Singhal, *Graduate Student Member, IEEE*, and Igor Paprotny, *Member, IEEE*

***Abstract*—Photonic crystals (PhCs) are periodically structured dielectric materials that have attracted significant research interest in the last two decades for their ability to slow down the group velocity of a propagating pulse envelope with promising sensing applications. This review article discusses the properties of 2-D PhCs including the slow-light phenomenon, bandgap generation, and application of these properties for gas and liquid sensing. Waveguide generation by introducing defects with light guiding and confinement is discussed. In addition, for 2-D PhC line waveguides, a comprehensive review on the slow-light principle and phenomenon of slow-light enhanced sensing for gases and liquids is discussed. 1-D and 3-D PhCs are also reviewed for bandgap generation and defects in PhCs along with present fabrication challenges and future trends. Our study highlights an increase in the detection capabilities of PhC-based sensors paving way for high-sensitivity detectors with applications in ubiquitous monitoring of gases and liquids.**

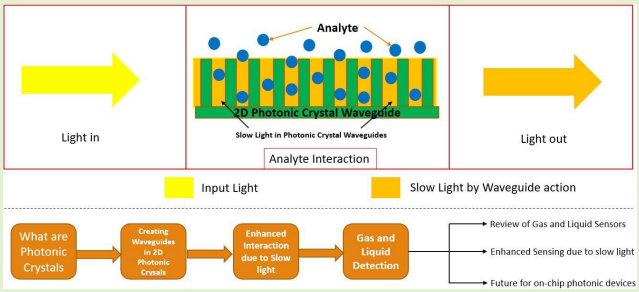

***Index Terms*—Gas sensing, liquid sensing, photonic bandgap (PBG), photonic crystals (PhCs), slow-light.**

Nomenclature

PhCs	Photonic crystals.
1-D	One-dimensional.
2-D	Two-dimensional.
3-D	Three-dimensional.
PBG	Photonic bandgap.
PhCW	Photonic crystal waveguides.

I. Introduction

PHCs can be naturally found in the exoskeleton of insects, wings, and feathers of birds, marine animals, and plants [1], [2], [3]. For example, 1-D PhCs occur in many species of butterflies [4], [5], [6], resulting in colored wings as shown in Fig. 1. Researchers have proposed a correlation between the periodicity of the structures and the wavelength of light attracting interest in artificially fabricated periodic structures to control light. The advancements in mechanical and electrical properties of metamaterials [7], [8], [9], [10], [11], [12] have motivated research for increased tuning of optical properties of PhCs. In the last two decades, significant effort has been put in to guide light in the desired direction and create perfectly reflecting surfaces and light confinement [13], [14]. Ever since their discovery, PhCs have found applications in telecommunications industry [15], [16], [17], electronic gates and polarizing filters [18], [19], [20], force sensing [21], antibiotic detection [22], and chemical sensing [23], [24].

Existing gas and liquid sensing technologies include metal-oxide (MOx) chemo-resistive sensors [25], [26]. For MOx gas sensors, continuous heating is required to start the surface chemisorption process, which can be energy intensive. 2-D materials and MOx-based gas sensors have been discussed by researchers [27], [28]. These sensors exhibit structural defects and material decay, which can adversely impact their reliability. Surface plasmon resonance (SPR)-based sensors have been widely reported for gas sensing [29], [30], [31] and biosensing [32], [33], [34], [35]. A reacting film sensitive to the target analyte is used to observe the SPR peak. These sensors need reactivation upon usage, and sensing mixtures could give false SPR peaks [36]

PhCs [38], [39], [40], [41], [42], [43], [44], [45], [46], [47] are aimed at engineering metamaterials that controls

Manuscript received 25 August 2022; accepted 29 August 2022. Date of publication 23 September 2022; date of current version 31 October 2022. The associate editor coordinating the review of this article and approving it for publication was Prof. Hsin-Ying Lee. *(Corresponding author: Igor Paprotny.)*

The authors are with the Micromechatronic Systems Laboratory, Department of Electrical and Computer Engineering, University of Illinois at Chicago, Chicago, IL 60607 USA (e-mail: asing48@uic.edu; paprotny@uic.edu).

Digital Object Identifier 10.1109/JSEN.2022.3205866

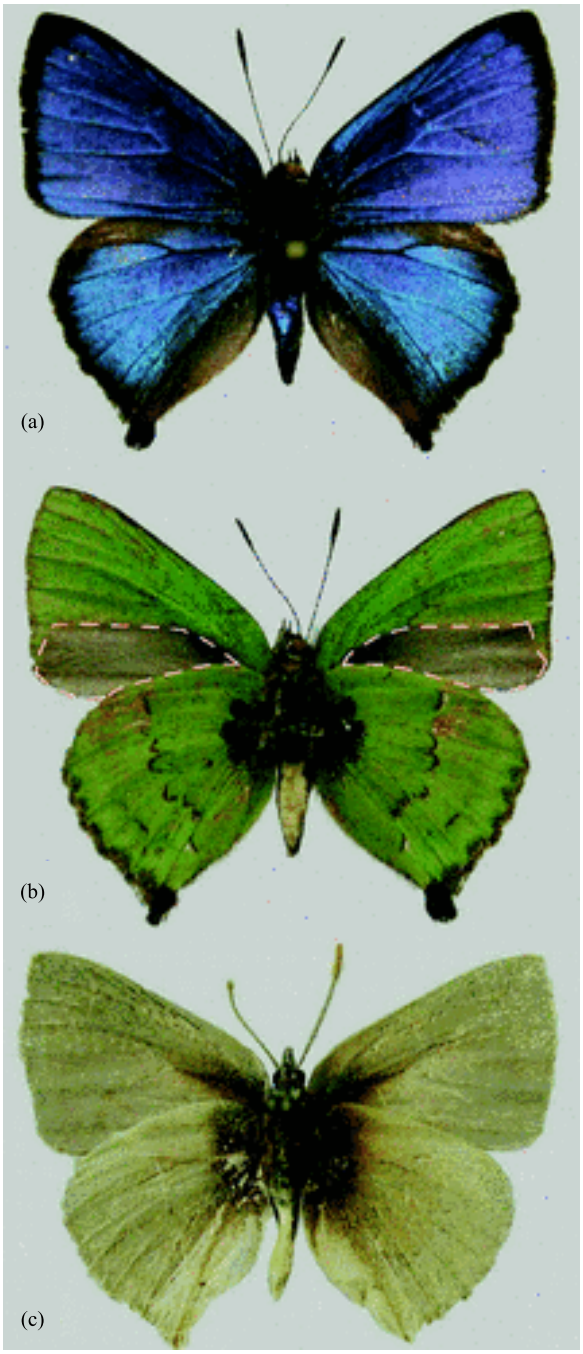

Fig. 1. (a) Dorsal surface and (b) ventral surface of the butterfly Cyanophrys remus showing their structural colors. (c) Ventral side of a bleached butterfly shown representing PhCs [37] [reproduced with permission].

the propagation of light. In electronic materials, atoms and molecules in a periodic arrangement with a pattern of repetition are known as crystal lattices. Electrons with certain energies are forbidden to propagate in a certain direction resulting in gaps or even complete bandgaps in the energy band structure. PhCs are optical analogs, materials with different dielectric constants replace atoms and molecules, and the periodic dielectric function replaces periodic potential. This allows for designing crystals with photonic bandgaps (PBGs), which prevents light with specific frequencies and directions from propagating.

A. Theoretical Bandgap Discussion

PhCs can be 1-D with periodicity and confinement in one direction, 2-D with periodicity and confinement in two directions, and 3-D with periodicity and confinement in all three directions [47]. The types of PhCs are shown in Fig. 2. In a 3-D PhC, a complete PBG is achieved [48], [49], [50]. A complete PBG is not achieved in a 1-D PhC as the material interface occurs only along one axis. The formation of PBG is understood by symmetries and electromagnetism. A continuous translation symmetric system is unchanged when a translation displacement d is introduced. Assuming that for each displacement d, the defined translation operator is t_d. The operator if operated on a function $p(r)$ will shift the argument by d. If the system is translationally invariant, then $t_d\epsilon(r) = \epsilon(r\text{-}d) = \epsilon(r)$, where $\epsilon(r)$ is the dielectric configuration. A continuous translation symmetry in the z-direction will be invariant under all of the $t_d's$ in z direction. The eigenfunction of any z-directional translate operator can be proved to be a mode with the functional form e^{ikz}

$$t_{dz}e^{\mathrm{ikz}} = e^{ik(z-d)} = \left(e^{-\mathrm{ikd}}\right)e^{\mathrm{ikz}} \tag{1}$$

where the eigenvalue is $e^{-\mathrm{ikd}}$. The modes of a z-directional system are eigenfunctions of any $t_d's$ which are classified as wave vectors k. These modes are lined up in ascending frequency for a given value of k. If the position of a mode's place in ascending frequency lineup is n, any mode can be defined by a unique name (k, n), where n is referred to as the band number. If the wave vector (k) versus mode frequency graph is plotted, n corresponds to different lines rising uniformly in frequency. Such a graph is referred to as *band structure.*

Like their electrical analogous, PhCs are not invariant for translations of any distance, but only a fixed step distance. This step length is called the lattice constant (a). This type of symmetry is called discrete translation symmetry, that is, $\epsilon(r) = \epsilon(r \pm a)$. The dielectric unit is considered a unit cell and the whole PhC is formed by a combination of multiple unit cells

$$H_k = e^{\mathrm{ikr}}u_k(r) = \left(r^{\mathrm{ikr}}\right)u_k(r+R). \tag{2}$$

A key feature that is derived from Bloch states is that not all values of k lead to a unique mode. Sometimes $k + G$ can lead to the same mode if G is the reciprocal lattice vector [51]. The wave vector specifies a phase relationship in different cells described by u. If k is incremented by G, then there will be an increment of GR in the phase between cells which is πN. Then incrementing k by G results in the same physical mode. Due to the redundancy in k, a restriction is made at a certain zone where the values of k outside this zone that otherwise is reached by adding G becomes redundant. These zones are called Brillouin zones and the zone closest to $k = 0$ is known as the first Brillouin zone [52], [53].

For waves propagating in the z-direction or perpendicular to the dielectric, only k_z is important. For the discussions in this review, we consider k_z as k. If three different multilayer films with different dielectric constant contrast are analyzed,

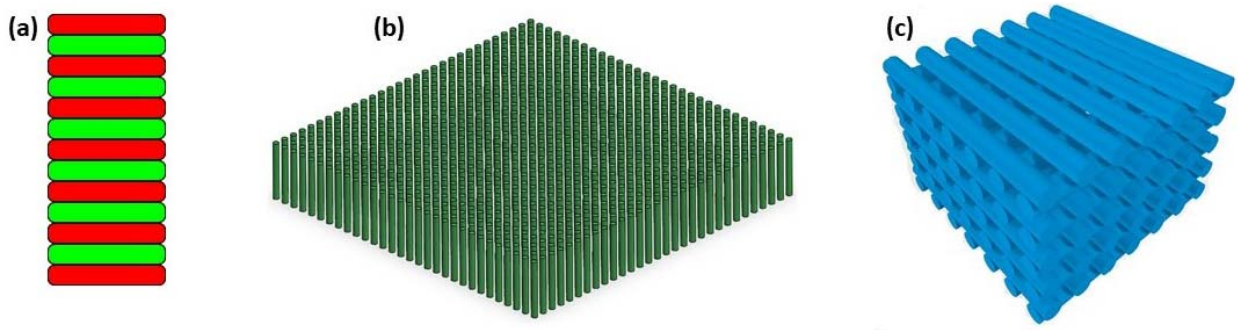

Fig. 2. Types of PhCs. (a) 1-D PhC with stack of varying dielectric materials. (b) 2-D PhC with dielectric pillars. (c) 3-D PhC with woodpile type structure.

it is observed that higher contrast in dielectric constants leads to a broader PBG as the low-frequency modes try to concentrate their energy where the dielectric constant is high, and similarly the high-frequency modes with respect to low dielectric constant. In 2-D or 3-D PhCs, the lower ϵ region is usually the air band.

In general, the range of frequencies prevented from the transmission is called PBG. On engineering a defect in a PhC, a guided mode is generated in the PBG which transmits the aligned wavelength of light at a lower group velocity. This is called slow-light phenomenon, and it results in enhanced sensing performance due to increased light–analyte interaction. This is further discussed in detail in Sections I-B and I-C.

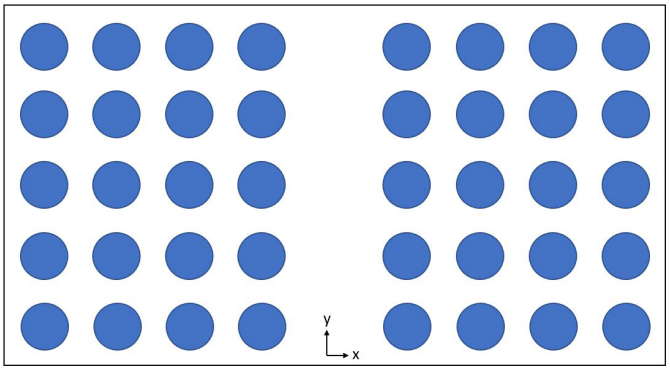

Fig. 3. Waveguide created by removing a column of rods (center) from a square lattice of rods.

B. Defects in PhCs

The addition of a defect in an otherwise perfect crystal creates a single localized mode that allows frequencies within the PBG. In 1-D PhCs, the defect is generated by varying the dielectric constant of one of the layers. In 2-D PhCs, a defect is created by removing a complete row or column from the perfect PhC leading to the formation of a waveguide or adding a perturbation in the size, dielectric constant, or shape. This disturbs the translational symmetry of the lattice resulting in modes appearing in the PBG. The defect mode generated behaves differently. If the propagation happens only in the plane of periodicity, the point defect is localized to a point in that plane. When a row or column is removed, it introduces a peak into the crystal's density of states in the PBG. The modes generated cannot penetrate the remaining crystal or outside the defect as it decays exponentially farther from the defect. This decay is visible as they are evanescent modes

$$H\,(r) = e^{ik_z} u\,(z)^{-k_z}\,. \tag{3}$$

In PBG, no electromagnetic modes are allowed. No real wave vectors exist for any mode of frequency in PBG. However, the modes are evanescent as they are complex and the amplitude decays exponentially farther from the defect.

A linear defect traps light and guides it within the defect. A light path also known as a waveguide is created in an otherwise perfect crystal by the introduction of a linear defect. In this system, the translational symmetry is preserved in one direction. For example, in the system shown in Fig. 3, the symmetry is preserved in the y-direction and continuous translational symmetry is preserved in the z-direction. For the analysis, only trasverse magnetic (TM) polarization is shown to consider in-plane propagation ($k_z = 0$). The band structure shows a guided mode in the PBG which also are all evanescent modes.

The difference between a point defect and a linear defect is that for a point defect, the mode is localized whenever its frequency lies in the PBG. However, for linear defects, the behavior of the mode is considered as a function of frequency and the wave vector k_y. If the conditions for chosen guided modes are not satisfied, they leak into the crystal and decay in the waveguide.

2-D periodic structures having a finite thickness are often known as PhC slabs or planar PhCs [54]. The finite thickness introduces a new behavior as the vertical wave vector k_z is not conserved anymore but due to the discrete translational symmetry in two directions, the in-plane wave vectors are conserved. The 2-D PhCs have two basic topologies: 1) rod-type PhCs [55], [56], [57] and 2) hole-type PhCs [45], [58], [59]. The basic structure for rod-type PhCs has dielectric rods forming a square lattice in the air. The air holes include a triangular lattice of air holes in a dielectric medium. An example of both topologies is shown in Fig. 4. The band diagrams (BD) for individual types are shown in Fig. 5. It is observed that the holes support transverse electric (TE)-like gaps, whereas the rods support TM-like gaps and none of the structures have a complete bandgap.

The thickness of the slab has a significant effect on the band structure. In a very thick slab, the bandgap disappears entirely and if the slab is too thin, the bands are weakly guided. This

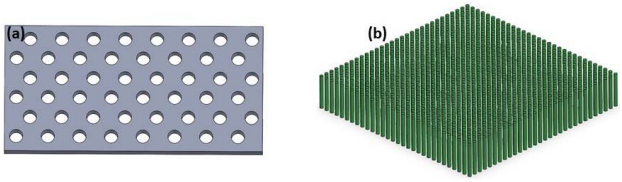

Fig. 4. Topologies for 2-D PhCWs. (a) Air hole type. (b) Rod types.

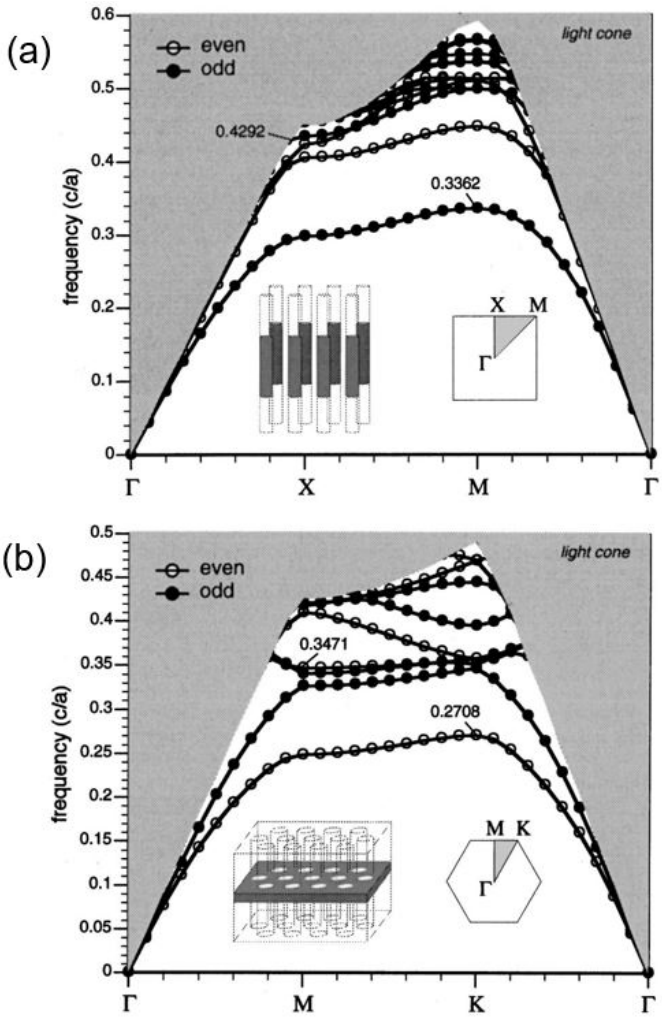

Fig. 5. Projected BD. (a) Rod-type and (b) air hole-type PhCs [60] [reproduced with permission].

allows the states lying just below the light line to decay slowly into the air region. This also makes the frequency difference between the light line and the lowest band too small to observe. If the slab is too thick, higher-order modes in the system are pulled down, which diminishes the bandgap. The design can be optimized for air volume and thickness to achieve wide PBG [61].

C. Slow-Light in PhCs

One of the properties that has attracted attention from a lot of researchers is the slow-light phenomenon [62]. The possible mechanism of slow-light is illustrated in Fig. 6. The light in the photonic crystal waveguide (PhCW) is coherently

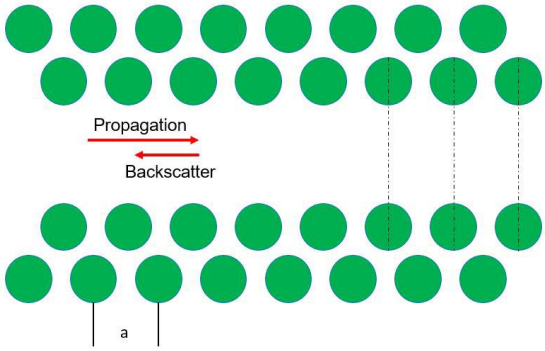

Fig. 6. Illustration of coherent scattering in PhCWs [62].

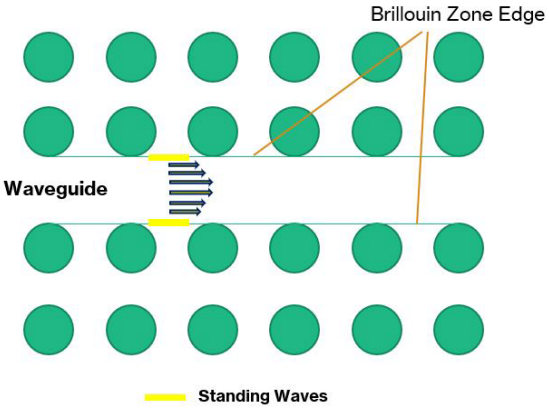

Fig. 7. Illustration of standing waves at the Brillouin zone edges and slowly moving waves in the area far away from the edge (midgap).

backscattered at each cell. At the Brillouin zone boundary, the backscattered light is in phase with the forward propagating light [62]. This introduces a standing wave that is a mode with zero group velocity. For the area away from the Brillouin zone boundary, both components no longer remain in phase and begin to move out of phase while interaction happens. To represent, the horizontal arrows in the image for propagating light are longer than the backscattered light. This results in a slow mode that is propagating in the forward direction.

This can also be understood using dispersion. The slope of dispersion or the group velocity goes to zero at the Brillouin zone edges which are the band edges. In a highly dispersive structure like PhCs, the band edge is the waveguide edge resulting in standing waves at the edges. For the area away from the Brillouin zone boundary, the standing waves are now slowly moving as shown in Fig. 7.

The phenomenon of group velocity dispersion has been discussed extensively [63], [64], [65], [66], [67]. In [63], Notomi *et al.* used a Fabry–Perot interferometer to analyze the dispersion and observe the oscillations and reported the oscillations becoming smaller as wavelength increases. The group index n_g for a mode propagating in a medium with refractive index n is given by $n_g = c/v_g$, where c is the speed of the light and v_g is the group velocity.

As the oscillations die, the group index increases, leading to a decrease in the group velocity. This phenomenon in PhCs

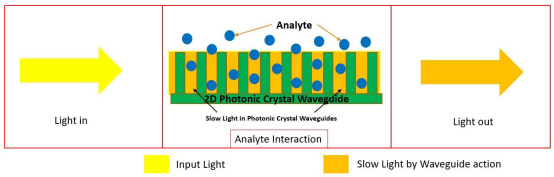

Fig. 8. Graphical representation of slow-light enhanced sensing using PhCs.

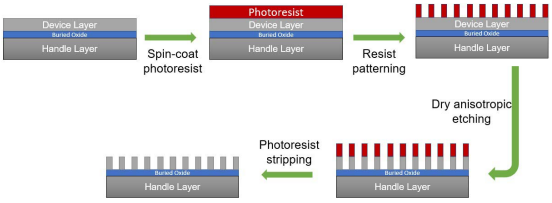

Fig. 9. Process to fabricate pillar-type 2-D PhCW.

leads to compressed optical path length which further reduces the size of the overall device or increases the light–matter interaction. By using PhCWs in optical sensors, the effective interaction path length is decreased without compensating the sensitivity.

The theoretical approach for absorption spectroscopy can be understood by Beer Lambert's law according to which the transmitted intensity is given as follow:

$$I = I_o e^{(-\gamma \alpha L)} \tag{4}$$

where I is the transmitted intensity, I_o is the incident light intensity, α is the absorption coefficient, L is the interaction length, and γ is the medium-specific absorption factor

$$\gamma = \frac{fc/n}{v_g}. \tag{5}$$

Here, v_g is the group velocity, f is the fill factor, c is speed of light, and n is the effective refractive index. For PhCs, the fill factor is high and by the slow-light phenomenon, the group velocity decreases leading to an increased absorption factor. As the group velocity decreases, the interaction between the analyte and light is enhanced [68]. Slow-light property of PhCs is discussed for improved gas sensing. For example, Kraeh *et al.* [69] discussed propene absorption using PhCW [69]. The slow-light tuning is possible for the mid-infrared (IR) range using dispersion engineering and thermo-optics which leads up to 20 nm of wavelength shift of the slow-light band edge [70]. Enhanced sensing due to slow light is also shown for biosensors [71]. The perturbation theory combined with the electromagnetic theory and Maxwell equations shows that achieving slow-light enhanced absorption is possible in microscale systems [54]. A graphical representation of slow-light sensing is shown in Fig. 8.

Linear defects in 2-D PhCs result in PhCW which shows a light phenomenon that leads to applications in gas and liquid sensing as discussed later in further sections. 1-D PhCs, as discussed, do not show PBG. A complete PBG is obtained in 3-D PhCs but the existing fabrication techniques are costly and time-consuming which have been discussed later in this review. This makes 2-D PhCs a promising platform for sensing. In this work, 2-D PhCs are discussed in detail for gas and liquid sensing.

D. Fabrication of PhCs

Fabrication of 2-D PhCW has been reported in the literature. A general process to fabricate a pillar-type PhC is illustrated in Fig. 9. The photoresist is spin-coated on a bare substrate, typically an silicon on insulator (SOI) wafer chosen to improve vertical light confinement [72], [73]. The photoresist is then patterned using different techniques like ultraviolet (UV) exposure [74], deep-UV exposure [75], e-beam exposure [76], and so on. The sample is then developed to expose the handle layer of the SOI substrate around the pillars. Dry anisotropic etching is used to etch the handle layer around the pillars [77]. Finally, the photoresist is stripped using dry or wet processes. This results in a 2-D pillar-type PhC. For a PhCW, a linear defect is generally introduced by removing a row of pillars at the lithography step. Advanced fabrication techniques for PhCs are discussed later in this review.

II. Sensing Using PhCWs

The increased interaction time between the analyte and the light in PhCWs results in enhanced absorption. The compact size promises a potential lab-on-a-chip gas sensing device. PhCWs can be designed with different lattice types. The triangular lattice is reported to have the widest bandgap [78]. The sensitivity of a PhC-based gas detection system depends largely on the light–analyte interactions. To utilize slow light completely, the PhCW is designed to maximize the reduction in the group velocity and observe a linear dispersion effect. There have been efforts to achieve low group velocity beyond the Brillouin zone edge. Researchers have reported modifications in the 2-D feature adjacent to the waveguide-like changes in radii, distance, and shape [79], [80], [81], [82], [83]. Numerical investigations on properties of waveguides were also reported [84], [85], [86].

PhC-based sensors can detect gases and liquids that have light absorption spectra in the operating range of the sensor. Distinct gases exhibit absorption spectra at different wavelength ranges, for example, near-IR, mid-IR, or far-IR. As discussed, PhCs are designed to target a particular wavelength but are tunable by changing the lattice constant in agreement with the band structure [87], [88]. This allows the fabrication of PhC-based sensors to target different gases and liquids.

A. Gas Sensing

A PhCW can be used as a gas sensor by replacing the background air with the target gas. Slow light will enhance sensing, and large absorption can be achieved with small path lengths. Efforts for gas sensing using a PhCW have been summarized in Table I. PhCWs can be tuned to a target absorption line using structural changes, infiltration, and other techniques, which have been discussed further in this review.

A hexagonal lattice of silicon microtubes has been evaluated recently [69]. Solid pillars were used for 2-D PhCs but

TABLE I
2-D PHCW-BASED GAS SENSORS

Gas Detected	Sensitivity	Concentration	Detection Limit	Operating Wavelength	Measurement Cycle Time	Reference
C_3H_6	8.6 - 10.1%	-	-	5.3-5.6 μm	30 min	[69]
Acetylene	-	100%	1 ppm	1530 nm	-	[89]
CO	-	-	21.5 ppm	1568 nm	-	[90]
CO_2, CO, HCN	-	-	-	1550 - 1573 nm	-	[91]
-	300 nm/RIU	-	0.0001 RIU	1550 nm	-	[92]
CH_4	-	100 ppm	High PPBs	1665.5 nm	45 s	[93]
CO_2	-	-	20 ppm	5.4 μm - 6.78 μm	120	[94]
CO	-	3 ppm	125 ppb	4.55 μm	100 s	[95]
H_2S	1.2 X 10^4 nm/RIU	2-50 ppm	1.87 X 10^{-6} nm	1230 nm	-	[96]
Ethanol	11.7 % drop	-	500 ppb	3.4 μm	180 s	[97]
Ethanol	11.7 % drop	-	250 ppb	3.4 μm	180 s	[98]
CH_4	-	700 ppm	-	7.625 μm	-	[99]
NH_3	-	20 ppm	5 ppm	3 μm	-	[100]
CH_4	-	-	-	1653.7 nm	-	[101]
CO_2, CO, H_2S	-	-	1.56 ppm	1567- 1578 nm	-	[102]
Acetylene	660.77	-	-	1531 nm	20-30 s	[103]

fabricated hollow with 6.5-μm pitch, 80-μm height with a wall thickness of 300 nm. A controlled deposition technique for precise thickness was used. The target gas was propene (C_3H_6) with an absorption spectra between 5.3 and 5.6 μm of wavelength. For testing, after each cycle, N_2 was used to flush the chamber, and multiple cycles of the target gas were run for 30 min with a measurement frequency of 10 s. The authors report an average absorption of 8.6%–10.1%.

In another report, correlation spectroscopy and differential absorption were used to study a slotted PhC for the detection of acetylene [89]. Mathematically, it is shown that the sensitivity is related to the group index and the fill factor which confers the literature. The authors also discussed the optimization of the PhCW by using the BD of PhCW to enhance the slow-light effect over a wide range of wavelengths. The PhCW was created by introducing a linear defect in a triangular air hole structure on an SOI substrate. The defect region was made in a slot to increase light and acetylene interaction. The optimized structure has the position of the first and second rows of air holes next to the linear defect.

Carbon monoxide (CO) was detected using a triangular rod PhCW made from silicon with radius $r = 0.2a$, where a is the lattice constant [90]. A tapered lens fiber was used to connect the PhCW. The report also discusses the harmonics of lock-in amplifiers and methods to reduce the need for calibration. The operating wavelength was 1568 nm which is also an absorption line for CO. A sensor array based on the photonic crystals (PhCs) was also reported [91]. Tunable diode lasers are used for the detection of three different gases CO_2, CO, and hydrogen cyanide (HCN). The system had three different lasers with target wavelengths 1572.66, 1567, and 1550 nm targeting different gases. As the wavelengths are close, a single waveguide with square air holes lattice with a linear defect was used for the sensing. Lasers are switched with the gases. The system is reported to be functional for multiple fluids as well.

In another report by Kumar *et al.* [92], a different structure was proposed as shown in Fig. 10 where the radii of the holes adjacent to the linear defect were changed to form supercavities along the waveguide in an overall triangular air hole silicon-based crystal. The resonance wavelength for the supercavities was reported to be 1550 nm. The authors reported peak shifts with supercavities filled with the analyte.

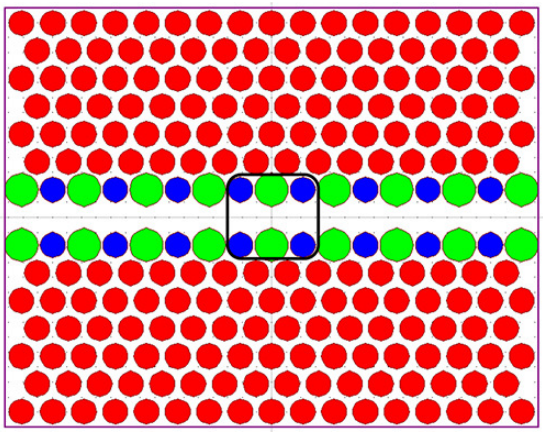

Fig. 10. Structure proposed for RI sensing [92] [reproduced with permission].

For methane sensing, a 300-μm long PhCW operating at a near-IR wavelength of 1670 nm is reported. It was fabricated on an SOI substrate. The group index was reported to decrease rapidly to 30% at 5 nm from the band edge [93]. The gas concentration for methane used was 100 ppm and good detection capabilities are reported.

An all-dielectric photonic crystal enhanced with a gas selective enrichment polymer polyethylenimine (PEI) capable of sensing CO_2 with a detection limit of 20 ppm and a response time of 2 min was also evaluated [94]. The PhC slab was fabricated on an SOI wafer with 500 nm of the device layer, and 1 μm of BOX and microfabrication techniques like e-beam lithography were used to define features. The PEI is diluted in deionized (DI) water (1:10) and then spin-coated on the surface.

The need for the low-loss cladding was discussed and a new substrate, silicon-on-sapphire (SoS), was introduced for applications to 5 μm of wavelength. The authors report a holey PhCW with a target wavelength of 4.55 μm used for the detection of carbon monoxide (CO) up to 3-ppm levels. At the response time of 75 s, a total of 14% drop is observed [95].

A graphene-modified PhC was tested as a hydrogen sulfide (H_2S) sensor with air holes in a triangular array on an SOI substrate [96]. The authors reported the deposition of graphene on the inner walls of the waveguide to increase the sensitivity toward H_2S. A sensitivity of 1.2×10^4 nm/RIU was reported.

A 9-mm long PhCW was described that allowed sensing ethyl alcohol at concentrations down to 500 ppb [97]. The authors reported an 11.7% of absorption drop observed on the introduction of gas in a PhCW made using an SOI platform. An updated work with a 250-ppb detection limit was also reported [98]. A 2-D rod-type PhCW was also discussed for methane (CH_4) detection in the mid-IR regime [99]. The finite difference time domain (FDTD) analysis was performed for a gas concentration of 700 ppm. A modification to the structure of the PhCW was also reported to optimize the PhC sensing.

A postfabrication technique was introduced to tune the slotted PhCW [104]. In this, the air slot was infiltrated with fluids of different refractive indices and the absorption was observed. The operating wavelength is 1550 nm. The reported shifts are reported in Table II.

For coupling, a resonant coupler was used to reduce the coupling losses. To increase the sensitivity, a PhC ring resonator based on a 2-D pillar hexagonal structure was created by removing the pillars [105]. In another effort, a PhCW surrounded by two ring linear defects made in a triangular air hole array was reported and a Fabry–Perot interference pattern was studied to calculate the sensitivity [106]. A new defect geometry, sunflower structure has also been explored [107]. The structure has air holes composed of high-density polyethylene. The sensor contained two symmetrical sample cells that surrounded the cavity in a circular PhC. FDTD analysis was done to find the response. A circular PhC was also reported with a sensitivity of 1054 nm/RIU [108].

Some reports of metallic PhCs are also available. 120-nm-thick tungsten trioxide deposited by thermal evaporation was used as a waveguide layer for hydrogen sensing fabricated on a glass substrate [109]. Gold nanowires were then laid on the overall layer. A theoretical limit of sub-ppm levels was reported.

Using different absorption wavelengths for analytes, detecting a mixture of gases with optical sensing has been previously shown [110], [111], [112]. As discussed earlier, PhCs can be designed to target different gases and liquids in isolation. PhCs can then further be used to detect mixtures of gases in a sensor array [113], [114]. Each waveguide targets a different gas in separation and a broadband source of light can be used to detect multiple gases. This enables applications in environmental gas sensing for PhC-based sensors.

B. Liquid Sensing

The increased light–matter interaction as explored for gas sensing also aids in sensing liquids. Optical techniques based on 2-D PhCWs are finding widespread applications in the detection of chemicals and other liquids [115], [116], [117], [118]. The increased emphasis on miniaturization of such systems also supports the lab-on-a-chip prototype for 2-D PhCWs. The liquid is generally introduced into the PhCW by drop coating for testing purposes which ensures a low volume requirement for the testing. In a slotted PhCW, a liquid with a different refractive index is introduced and as it fills the air holes, the overall refractive index is changed. The PBG will in turn be affected by the refractive index of the introduced liquid. Similar to gas sensors, liquid sensors can also be tuned to target the wavelength.

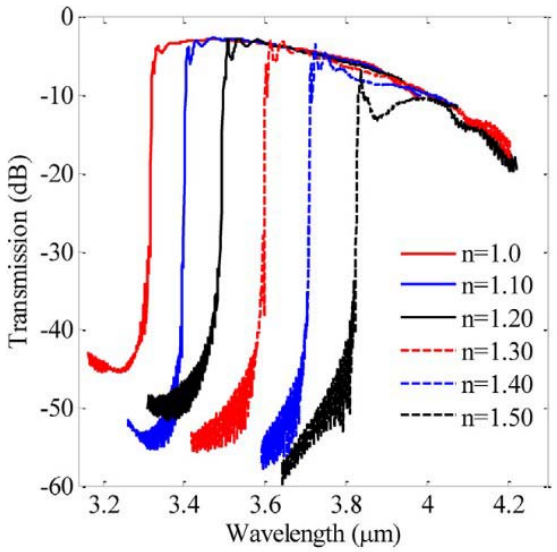

Fig. 11. Shift in wavelength with the change in the refractive index of the analyte [121] [reproduced with permission].

Slotted PhCWs were designed for mid-IR refractive index sensing, and wavelength shift was observed [121]. For refractive-index sensing, the shift is shown in Fig. 11. PhCWs were tested using varying refractive index and plane wave expansion (PWE) [123] and 3-D FDTD [122]. The refractive indices from 1 to 1.5 were tested and a band diagram was observed. Both reports test for changes at 1550 nm of wavelength and reports good sensitivity for a triangular PhCW.

Topol'ančik *et al.* [115] introduced two different defects in the crystal creating a multichannel sensing platform to detect more than one liquid. The PhCWs were fabricated in the gallium arsenide (GaAs) substrate, and the response for xylene and isopropanol was demonstrated with good sensitivity.

Variation in refractive index by infiltration was also analyzed [124]. In a triangular air-hole PhCW made on a silicon substrate, the radii of air holes localized at each side of the waveguide were optimized and infiltrated to increase the sensitivity.

Other designs have also been evaluated for refractive index sensing that can be used as liquid sensors including a circular PhC was reported with a sensitivity of 1054 nm/RIU [108]. A T-shaped PhC was evaluated, and the highest sensitivity of 1040 nm/RIU was reported [125]. The efforts for sensing liquids are summarized in Table III. The results in the literature are a confirmation of the theory making 2-D PhCWs a strong method for lab-on-a-chip liquid sensing.

C. Discussion

The slow-light property of PhCs has a tremendous advantage because the light–analyte interaction can be enhanced significantly by reducing the path length resulting in a potential

TABLE II
UP AND BOTTOM EDGE, WIDTH OF PBG, AND GUIDED MODE EDGE FOR THE VARIATION OF THE INFILTRATED FLUID REFRACTIVE INDEX IN THE SLOTTED PHCW [104] [REPRODUCED WITH PERMISSION]

n_f	Bottom Edge (nm)	Up Edge (nm)	Width of PBG (nm)	Guided Mode Edge (nm)
1.00	1966.02	1371.74	594.28	1532.49
1.50	1966.03	1378.28	587.76	1571.13
1.55	1966.04	1379.62	586.41	1579.16
1.60	1966.04	1380.98	585.05	1587.27
1.65	1966.04	1386.01	580.03	1595.45
1.70	1966.04	1393.15	572.89	1603.71

TABLE III
2-D PHCW-BASED LIQUID SENSORS. LIQUID SAMPLES ARE INTRODUCED VIA MEASURES LIKE DROPPER, AND SO ON, WHICH DOES NOT ALLOW MEASUREMENT TIME CALCULATIONS

Chemical Detected	Sensitivity	Operating Wavelength	Reference
IPA, Xylene	-	1500 - 1620 nm	[115]
C_6H_{12}, CCl_4	35 dB/n	67-110 GHz	[116]
Water, Sugar Solution	700 nm/RIU	1300-1600 nm	[117]
Water, IPA, Ethanol	110 nm/RIU	1520-1620 nm	[118]
-	636 nm/RIU	1450 - 2000 nm	[119]
Caster Sugar	1500	1550 nm	[120]
Ethylene Glycol	1150 nm/RIU	3.6 μm	[121]
Liquids (n=1.0 to 1.5)	200 nm/RIU	1550 nm	[122]
Liquids (n=1.0 to 1.5)	$2.3x10^9 nm/RIU$	1550 nm	[123]

lab-on-a-chip sensor for gas and liquid detection. Slow-light properties can also be tuned to the desired wavelength using infiltration, structural changes, and material properties. This review outlined multiple works on slow-light tuning for a target wavelength. Applications in visible, near IR-, mid-IR spectra are possible and have been discussed in this review.

Linear defects used to create PhCWs can also be tuned by changing the structural parameters and have been widely utilized to fabricate sensors. Dispersion is frequently used to enhance the bandpass operation [63], [64], [65], [66], [67]. Fabrication of such structures involves planar microfabrication techniques, focused ion-beam, and e-beam lithography. These techniques are often time-consuming and costly. Fabrication complexity is also increased for applications in visible spectra as the feature size is reduced to sub-500 nm. PBG and signal strength are critically dependent on the structural parameters and even a small deviation in the size of structures results in a target peak shift. Precise fabrication of the PhCW structure is essential for transmission strength as defects can result in undesired attenuation of light.

Signal attenuation also increases with coupling mismatch at the entry and exit of light from PhCWs. Optical fiber cores usually have a diameter of 8–10 μm, much higher than the PhCs resulting in a modal mismatch at the interface of PhCs and optical fibers. Many techniques have been evaluated to improve the modal mismatch, for example [126], and have also been summarized [127]. The advancements in fabrication and interfacing technology guide in the direction of large-scale operation of PhCs enabling full potential use with efficient applications.

III. FUTURE DIRECTION

Along with the properties discussed in the review, PhCs have other properties that have received great interest among researchers. This includes low-loss sharp PhCW bends up to 120° have been successfully achieved [128]. This enables directing light to the desired path which can be further useful for light splitting [129]. The PhCs also exhibit the superprism phenomenon which further enables microscale light circuits in silicon [41], [130].

Apart from 2-D PhCs, there are reports on both 1-D and 3-D PhCs with some advantages and disadvantages over 2-D PhCs. 1-D PhCs have been utilized for various applications due to the ease of fabrication and low costs. The researchers have also targeted the omnidirectional bands [131], [132], [133]. Tolmachev *et al.* [134] discussed the design of 1-D PhCs using a combination of bandgaps and gap map (GM) approaches and demonstrated modeling of PhCs using both forbidden GM methods and BD.

There have been many reports using 1-D PhCs for different applications. Bouzidi *et al.* [135] used 1-D PhCs with magnesium fluoride and silicon alternating layers with an empty layer in between which is filled with the gas to be tested. The sensitivity of 700 nm/RIU was reported.

Many other materials were also used for creating 1-D PhC-based sensors. Clevenson *et al.* [136] reported a high-Q

suspended polymer PhC nanocavity implemented in a flexible polymer which swells on interaction with target gas. The experimental sensitivity was reported to be 10 ppm. A multilayer approach has also been used and a theoretical model has been discussed including the effect of a number of periods, changes in the gas refractive index, the effect of layer thickness, incident angle, prism thickness, and so on [137].

3-D PhCs have the advantage over both 1-D and 2-D PhCs that they can provide a complete bandgap resulting in a larger stopband and increased sensitivity. Despite all the features, 3-D PhCs are not common as fabricating precise structures is a relatively difficult task. By using the conventional microfabrication techniques, a woodpile structure can be fabricated consisting of 1-D rods arranged in a stacking sequence by using repetitive deposition and etching. Lin *et al.* [138] reported a 3-D PhC made using the traditional techniques with SiO2 as a support structure and depositing polysilicon resulting in a structure exhibiting very large PBG. Constant efforts for new fabrication techniques are being made to fabricate 3-D PhCs easily without any support structures. Takahashi *et al.* [139] reported a direct creation top-down approach for fabrication of 3-D PhCs by double-angled deep etching method enabling the direct creation of 3-D structures in single-crystalline silicon. Defects can also be introduced into 3-D PhCs like the 2-D crystals to control the light [140].

To further ease the fabrication process for 3-D PhCs, two-photon polymerization-based lithography has been explored by the researchers [141], [142], [143]. In two-photon polymerization, a femtosecond laser is used and is tightly focused on a photosensitive resin through an objective lens with a high numerical aperture. The objective usually dips in the resin and exposes the resist. Using two-photon polymerization, a 3-D PhC was fabricated out of SU-8 which has a very low refractive index contrast to the target gases. Postprocessing was used to fabricate high-refractive index crystals [144].

IV. Conclusion

In this review, a thorough study of slow-light enhanced liquid and gas sensing has been carried out for line waveguides in 2-D PhCs. Reported work and correlation of results demonstrate that slow light can significantly increase the sensing capability of a PhCW. Various PhCWs, their structure, sensitivity, fabrication, and slow-light mechanism have been discussed in detail. The availability of slow light largely depends on structural and material characteristics which can be tuned to the desired wavelength enabling targeted sensing. It is likely that PhC-based technology will enable future integration of on-chip photonic devices, microfluidic sensing of liquids and gases with further reduced path lengths, and enabling new possibilities for on-chip integrated highly sensitive gas and liquid sensors.

References

[1] J. W. Galusha, L. R. Richey, M. R. Jorgensen, J. S. Gardner, and A. H. Bartl, "Study of natural photonic crystals in beetle scales and their conversion into inorganic structures via a sol–gel bio-templating route," *J. Mater. Chem.*, vol. 20, no. 7, pp. 1277–1284, 2010.

[2] J. P. Vigneron and P. Simonis, "Natural photonic crystals," *Phys. B, Condens. Matter*, vol. 407, no. 20, pp. 4032–4036, 2012.

[3] D. Comoretto *et al.*, *Organic and Hybrid Photonic Crystals*. Switzerland: Springer, 2015.

[4] R. P. Zaccaria, "Butterfly wing color: A photonic crystal demonstration," *Opt. Lasers Eng.*, vol. 76, pp. 70–73, Jan. 2016.

[5] L. P. Biró *et al.*, "Living photonic crystals: Butterfly scales—Nanostructure and optical properties," *Mater. Sci. Eng., C*, vol. 27, nos. 5–8, pp. 941–946, Sep. 2007.

[6] Z. Vértesy, Z. Bálint, K. Kertész, J. P. Vigneron, V. Lousse, and L. P. Biró, "Wing scale microstructures and nanostructures in butterflies–natural photonic crystals," *J. Microsc.*, vol. 224, no. 1, pp. 108–110, Oct. 2006.

[7] T. Hlasek *et al.*, "Enhanced mechanical properties of single-domain YBCO bulk superconductors processed with artificial holes," *IEEE Trans. Appl. Supercond.*, vol. 29, no. 5, pp. 1–4, Aug. 2019.

[8] Z. Li *et al.*, "Enhanced mechanical properties of graphene (reduced graphene oxide)/aluminum composites with a bioinspired nanolaminated structure," *Nano Lett.*, vol. 15, no. 12, pp. 8077–8083, Dec. 2015.

[9] C.-C. Wang, J.-F. Song, H.-M. Bao, Q.-D. Shen, and C.-Z. Yang, "Enhancement of electrical properties of ferroelectric polymers by polyaniline nanofibers with controllable conductivities," *Adv. Funct. Mater.*, vol. 18, no. 8, pp. 1299–1306, Apr. 2008.

[10] R. Z. Valiev, M. Y. Murashkin, and I. Sabirov, "A nanostructural design to produce high-strength al alloys with enhanced electrical conductivity," *Scripta Mater.*, vol. 76, pp. 13–16, Apr. 2014.

[11] M. Y. Murashkin, I. Sabirov, V. U. Kazykhanov, E. V. Bobruk, A. A. Dubravina, and R. Z. Valiev, "Enhanced mechanical properties and electrical conductivity in ultrafine-grained al alloy processed via ECAP-PC," *J. Mater. Sci.*, vol. 48, no. 13, pp. 4501–4509, Jul. 2013.

[12] C. Liu, J. Chen, Y. Lai, D. Zhu, Y. Gu, and J. Chen, "Enhancing electrical conductivity and strength in al alloys by modification of conventional thermo-mechanical process," *Mater. Des.*, vol. 87, pp. 1–5, Dec. 2015.

[13] M. Notomi, "Manipulating light with strongly modulated photonic crystals," *Rep. Prog. Phys.*, vol. 73, no. 9, Aug. 2010, Art. no. 096501.

[14] H. Benisty *et al.*, "Optical and confinement properties of two-dimensional photonic crystals," *J. Lightw. Technol.*, vol. 17, no. 11, pp. 2063–2077, Nov. 1999.

[15] A. Reutlinger *et al.*, "Fiber optic sensing for telecommunication satellites," *Proc. SPIE*, vol. 10566, Nov. 2017, Art. no. 105661C.

[16] P. Sharma, S. Pardeshi, R. K. Arora, and M. Singh, "A review of the development in the field of fiber optic communication systems," *Int. J. Emerg. Technol. Adv. Eng.*, vol. 3, no. 5, pp. 113–119, 2013.

[17] A. Willner, *Optical Fiber Telecommunications*, vol. 11. New York, NY, USA: Academic, 2019.

[18] V. S. Chaudhary, D. Kumar, and S. Kumar, "SPR-assisted photonic crystal fiber-based dual-wavelength single polarizing filter with improved performance," *IEEE Trans. Plasma Sci.*, vol. 49, no. 12, pp. 3803–3810, Dec. 2021.

[19] D. G. S. Rao, S. Swarnakar, and S. Kumar, "Design of all-optical reversible logic gates using photonic crystal waveguides for optical computing and photonic integrated circuits," *Appl. Opt.*, vol. 59, no. 35, pp. 11003–11012, 2020.

[20] D. G. S. Rao, S. Swarnakar, and S. Kumar, "Design of photonic crystal based compact all-optical 2×1 multiplexer for optical processing devices," *Microelectron. J.*, vol. 112, Jun. 2021, Art. no. 105046.

[21] T. Sreenivasulu, V. Rao, T. Badrinarayana, G. Hegde, and T. Srinivas, "Photonic crystal ring resonator based force sensor: Design and analysis," *Optik*, vol. 155, pp. 111–120, Feb. 2018.

[22] H. Yan *et al.*, "Specific detection of antibiotics by silicon-on-chip photonic crystal biosensor arrays," *IEEE Sensors J.*, vol. 17, no. 18, pp. 5915–5919, Sep. 2017.

[23] C. Fenzl, T. Hirsch, and O. S. Wolfbeis, "Photonic crystals for chemical sensing and biosensing," *Angew. Chem. Int. Ed.*, vol. 53, no. 13, pp. 3318–3335, Mar. 2014.

[24] X. Xu, A. V. Goponenko, and S. A. Asher, "Polymerized PolyHEMA photonic crystals: PH and ethanol sensor materials," *J. Amer. Chem. Soc.*, vol. 130, no. 10, pp. 3113–3119, Mar. 2008.

[25] P. Fau *et al.*, "Nanosized tin oxide sensitive layer on a silicon platform for domestic gas applications," *Sens. Actuators B, Chem.*, vol. 78, nos. 1–3, pp. 83–88, Aug. 2001.

[26] D. Barreca *et al.*, "1D ZnO nano-assemblies by plasma-CVD as chemical sensors for flammable and toxic gases," *Sens. Actuators B, Chem.*, vol. 149, no. 1, pp. 1–7, Aug. 2010.

[27] M. T. Humayun *et al.*, "Ubiquitous low-cost functionalized multi-walled carbon nanotube sensors for distributed methane leak detection," *IEEE Sensors J.*, vol. 16, no. 24, pp. 8692–8699, Dec. 2016.

[28] J. Xiang, A. Singhal, R. Divan, L. Stan, Y. Liu, and I. Paprotny, "Selective volatile organic compound gas sensor based on carbon nanotubes functionalized with ZnO nanoparticles," *J. Vac. Sci. Technol. B*, vol. 39, no. 4, Jul. 2021, Art. no. 042803.

[29] D. Li *et al.*, "Molybdenum disulfide nanosheets deposited on polished optical fiber for humidity sensing and human breath monitoring," *Opt. Exp.*, vol. 25, no. 23, pp. 28407–28416, 2017.

[30] A. Nooke *et al.*, "On the application of gold based SPR sensors for the detection of hazardous gases," *Sens. Actuators B, Chem.*, vol. 149, no. 1, pp. 194–198, Aug. 2010.

[31] A. Paliwal, A. Sharma, M. Tomar, and V. Gupta, "Carbon monoxide (CO) optical gas sensor based on ZnO thin films," *Sens. Actuators B, Chem.*, vol. 250, pp. 679–685, Oct. 2017.

[32] V. S. Chaudhary, D. Kumar, and S. Kumar, "Gold-immobilized photonic crystal fiber-based SPR biosensor for detection of malaria disease in human body," *IEEE Sensors J.*, vol. 21, no. 16, pp. 17800–17807, Aug. 2021.

[33] R. Srivastava, Y. K. Prajapati, S. Pal, and S. Kumar, "Micro-channel plasmon sensor based on a D-Shaped photonic crystal fiber for malaria diagnosis with improved performance," *IEEE Sensors J.*, vol. 22, no. 15, pp. 14834–14841, Aug. 2022.

[34] Z. Wang, R. Singh, C. Marques, R. Jha, B. Zhang, and S. Kumar, "Taper-in-taper fiber structure-based LSPR sensor for alanine aminotransferase detection," *Opt. Exp.*, vol. 29, no. 26, pp. 43793–43810, Dec. 2021.

[35] V. S. Chaudhary, D. Kumar, G. P. Mishra, S. Sharma, and S. Kumar, "Plasmonic biosensor with gold and titanium dioxide immobilized on photonic crystal fiber for blood composition detection," *IEEE Sensors J.*, vol. 22, no. 9, pp. 8474–8481, May 2022.

[36] J.-H. Park, Y.-W. Cho, and T.-H. Kim, "Recent advances in surface plasmon resonance sensors for sensitive optical detection of pathogens," *Biosensors*, vol. 12, no. 3, p. 180, Mar. 2022.

[37] K. Kertész *et al.*, "Gleaming and dull surface textures from photonic-crystal-type nanostructures in the butterflyCyanophrys remus," *Phys. Rev. E, Stat. Phys. Plasmas Fluids Relat. Interdiscip. Top.*, vol. 74, no. 2, Aug. 2006, Art. no. 021922.

[38] E. Yablonovitch, "Photonic crystals," *J. Modern Opt.*, vol. 41, no. 2, pp. 173–194, 1994.

[39] J. D. Joannopoulos, P. R. Villeneuve, and S. Fan, "Photonic crystals: Putting a new twist on light," *Nature*, vol. 386, no. 6621, pp. 143–149, Mar. 1997.

[40] J.-M. Lourtioz, H. Benisty, V. Berger, J.-M. Gerard, D. Maystre, and A. Tchelnokov, "Photonic crystals," in *Towards Nanoscale Photonic Devices*. Berlin, Germany: Springer-Verlag, 2005.

[41] H. Kosaka *et al.*, "Superprism phenomena in photonic crystals," *Phys. Rev. B, Condens. Matter*, vol. 58, no. 16, pp. R10096–R10099, Oct. 1998.

[42] K. Sakoda, *Optical Properties of Photonic Crystals*, vol. 80. Berlin, Germany: Springer, 2004.

[43] D. Prather, "Photonic crystals: An engineering perspective," *Opt. Photon. News*, vol. 13, no. 6, pp. 16–19, 2002.

[44] S. G. Johnson and J. D. Joannopoulos, *Photonic Crystals: The Road From Theory to Practice*. USA: Springer, 2001.

[45] S. Noda and T. Baba, *Roadmap on Photonic Crystals*, vol. 1. USA: Springer, 2003.

[46] T. F. Krauss and M. Richard, "Photonic crystals in the optical regime-past, present and future," *Prog. Quantum Electron.*, vol. 23, no. 2, pp. 51–96, 1999.

[47] K. Inoue and K. Ohtaka, *Photonic Crystals: Physics, Fabrication and Applications*, vol. 94. USA: Springer, 2004.

[48] J. G. Fleming *et al.*, "All-metallic three-dimensional photonic crystals with a large infrared bandgap," *Nature*, vol. 417, pp. 52–55, May 2002.

[49] S. Wong *et al.*, "Direct laser writing of three-dimensional photonic crystals with a complete photonic bandgap in chalcogenide glasses," *Adv. Mater.*, vol. 18, no. 3, pp. 265–269, Feb. 2006.

[50] J. Schilling and A. Scherer, "3D photonic crystals based on macroporous silicon: Towards a large complete photonic bandgap," *Photon. Nanostruct. Fundamentals Appl.*, vol. 3, nos. 2–3, pp. 90–95, Dec. 2005.

[51] J. D. Joannopoulos, S. G. Johnson, J. N. Winn, and R. D. Meade, *Photonic Crystals*. Princeton, NJ, USA: Princeton Univ. Press, 2011.

[52] J. Witzens, M. Loncar, and A. Scherer, "Self-collimation in planar photonic crystals," *IEEE J. Sel. Topics Quantum Electron.*, vol. 8, no. 6, pp. 1246–1257, Nov. 2002.

[53] D. N. Chigrin, S. Enoch, C. M. S. Torres, and G. Tayeb, "Self-guiding in two-dimensional photonic crystals," *Opt. Exp.*, vol. 11, no. 10, pp. 1203–1211, 2003.

[54] J. D. Joannopoulos, S. G. Johnson, J. N. Winn, and R. D. Meade, *Molding the Flow of Light*. Princeton, NJ, USA: Princeton Univ. Press, 2008.

[55] V. V. Poborchii, T. Tada, and T. Kanayama, "Si pillar photonic crystal slab with linear defects: Transmittance and waveguide properties," *Opt. Commun.*, vol. 210, nos. 3–6, pp. 285–290, Sep. 2002.

[56] V. Poborchii, T. Tada, T. Kanayama, and A. Moroz, "Silver-coated silicon pillar photonic crystals: Enhancement of a photonic band gap," *Appl. Phys. Lett.*, vol. 82, no. 4, pp. 508–510, Jan. 2003.

[57] X. Ao, L. Liu, L. Wosinski, and S. He, "Polarization beam splitter based on a two-dimensional photonic crystal of pillar type," *Appl. Phys. Lett.*, vol. 89, no. 17, Oct. 2006, Art. no. 171115.

[58] T. Yoshie, J. Vučković, A. Scherer, H. Chen, and D. Deppe, "High quality two-dimensional photonic crystal slab cavities," *Appl. Phys. Lett.*, vol. 79, no. 26, pp. 4289–4291, Dec. 2001.

[59] Y. Tanaka, T. Asano, Y. Akahane, B.-S. Song, and S. Noda, "Theoretical investigation of a two-dimensional photonic crystal slab with truncated cone air holes," *Appl. Phys. Lett.*, vol. 82, no. 11, pp. 1661–1663, Mar. 2003.

[60] S. G. Johnson, P. R. Villeneuve, S. Fan, and J. D. Joannopoulos, "Linear waveguides in photonic-crystal slabs," *Phys. Rev. B, Condens. Matter*, vol. 62, no. 12, p. 8212, 2000.

[61] J. Hou, D. S. Citrin, H. Wu, D. Gao, Z. Zhou, and S. Chen, "Slab-thickness dependence of photonic bandgap in photonic-crystal slabs," *IEEE J. Sel. Topics Quantum Electron.*, vol. 18, no. 6, pp. 1636–1642, Nov. 2011.

[62] T. F. Krauss, "Slow light in photonic crystal waveguides," *J. Phys. D, Appl. Phys.*, vol. 40, no. 9, p. 2666, 2007.

[63] M. Notomi, K. Yamada, A. Shinya, J. Takahashi, C. Takahashi, and I. Yokohama, "Extremely large group-velocity dispersion of line-defect waveguides in photonic crystal slabs," *Phys. Rev. Lett.*, vol. 87, no. 25, Nov. 2001, Art. no. 253902.

[64] A. Martínez, A. García, P. Sanchis, and J Martí, "Group velocity and dispersion model of coupled-cavity waveguides in photonic crystals," *J. Opt. Soc. Amer. A, Opt. Image Sci.*, vol. 20, no. 1, pp. 147–150, 2003.

[65] A. Imhof, W. L. Vos, R. Sprik, and A. Lagendijk, "Large dispersive effects near the band edges of photonic crystals," *Phys. Rev. Lett.*, vol. 83, no. 15, p. 2942, 1999.

[66] M. Galli, D. Bajoni, F. Marabelli, L. C. Andreani, L. Pavesi, and G. Pucker, "Photonic bands and group-velocity dispersion in Si/SiO_2 photonic crystals from white-light interferometry," *Phys. Rev. B, Condens. Matter*, vol. 69, no. 11, Mar. 2004, Art. no. 115107.

[67] G. von Freymann, S. John, S. Wong, V. Kitaev, and G. A. Ozin, "Measurement of group velocity dispersion for finite size three-dimensional photonic crystals in the near-infrared spectral region," *Appl. Phys. Lett.*, vol. 86, no. 5, Jan. 2005, Art. no. 053108.

[68] N. A. Mortensen and S. Xiao, "Slow-light enhancement of Beer-Lambert-Bouguer absorption," *Appl. Phys. Lett.*, vol. 90, no. 14, Apr. 2007, Art. no. 141108.

[69] C. Kraeh, J. L. Martinez-Hurtado, A. Popescu, H. Hedler, and J. J. Finley, "Slow light enhanced gas sensing in photonic crystals," *Opt. Mater.*, vol. 76, pp. 106–110, Feb. 2018.

[70] Y. Ma, B. Dong, B. Li, K.-W. Ang, and C. Lee, "Dispersion engineering and thermo-optic tuning in mid-infrared photonic crystal slow light waveguides on silicon-on-insulator," *Opt. Lett.*, vol. 43, no. 22, pp. 5504–5507, 2018.

[71] W.-C. Lai, S. Chakravarty, Y. Zou, Y. Guo, and R. T. Chen, "Slow light enhanced sensitivity of resonance modes in photonic crystal biosensors," *Appl. Phys. Lett.*, vol. 102, no. 4, Jan. 2013, Art. no. 041111.

[72] M. Lončar, T. Doll, J. Vučković, and A. Scherer, "Design and fabrication of silicon photonic crystal optical waveguides," *J. Lightw. Technol.*, vol. 18, no. 10, p. 1402, Oct. 1, 2000.

[73] S. Yliniemi *et al.*, "Fabrication of photonic crystal waveguide elements on SOI," *Proc. SPIE*, vol. 4944, pp. 23–31, Apr. 2003.

[74] M. Belotti *et al.*, "Fabrication of SOI photonic crystal slabs by soft UV-nanoimprint lithography," *Microelectronic Eng.*, vol. 83, nos. 4–9, pp. 1773–1777, Apr. 2006.

[75] W. Bogaerts *et al.*, "Fabrication of photonic crystals in silicon-on-insulator using 248-nm deep UV lithography," *IEEE J. Sel. Topics Quantum Electron.*, vol. 8, no. 4, pp. 928–934, Jul. 2002.

[76] L. H. Frandsen *et al.*, "Topology optimized mode conversion in a photonic crystal waveguide fabricated in silicon-on-insulator material," *Opt. Exp.*, vol. 22, no. 7, pp. 8525–8532, Apr. 2014.

[77] T. Zijlstra, E. V. D. Drift, M. D. Dood, E. Snoeks, and A. Polman, "Fabrication of two-dimensional photonic crystal waveguides for 1.5 μm in silicon by deep anisotropic dry etching," *J. Vac. Sci. Technol. B, Microelectron. Nanometer Struct. Process., Meas., Phenomena*, vol. 17, no. 6, pp. 2734–2739, 1999.

[78] R. Wang, X.-H. Wang, B.-Y. Gu, and G.-Z. Yang, "Effects of shapes and orientations of scatterers and lattice symmetries on the photonic band gap in two-dimensional photonic crystals," *J. Appl. Phys.*, vol. 90, no. 9, pp. 4307–4313, Nov. 2001.

[79] Y.-N. Zhang, Y. Zhao, and Q. Wang, "Optimizing the slow light properties of slotted photonic crystal waveguide and its application in a high-sensitivity gas sensing system," *Meas. Sci. Technol.*, vol. 24, no. 10, Oct. 2013, Art. no. 105109.

[80] A. Di Falco, L. O'Faolain, and T. F. Krauss, "Dispersion control and slow light in slotted photonic crystal waveguides," *Appl. Phys. Lett.*, vol. 92, no. 8, Feb. 2008, Art. no. 083501.

[81] K.-T. Zhu, T.-S. Deng, Y. Sun, Q.-F. Zhang, and J.-L. Wu, "Slow light property in ring-shape-hole slotted photonic crystal waveguide," *Opt. Commun.*, vol. 290, pp. 87–91, Mar. 2013.

[82] C. Bao *et al.*, "Low dispersion slow light in slot waveguide grating," *IEEE Photon. Technol. Lett.*, vol. 23, no. 22, pp. 1700–1702, Nov. 15, 2011.

[83] A. Benmerkhi, M. Bouchemat, and T. Bouchemat, "Influence of elliptical shaped holes on the sensitivity and q factor in 2D photonic crystals sensor," *Photon. Nanostruct. Fundamentals Appl.*, vol. 20, pp. 7–17, Jul. 2016.

[84] S.-Y. Lin, E. Chow, V. Hietala, P. R. Villeneuve, and J. D. Joannopoulos, "Experimental demonstration of guiding and bending of electromagnetic waves in a photonic crystal," *Science*, vol. 282, no. 5387, pp. 274–276, Oct. 1998.

[85] C. Ranacher, C. Consani, R. Jannesari, T. Grille, and A. Jakoby, "Numerical investigations of infrared slot waveguides for gas sensing," *Multidisciplinary Digit. Publishing Inst. Proc.*, vol. 2, p. 799, 2018.

[86] V. Zabelin, "Numerical investigations of two-dimensional photonic crystal optical properties, design and analysis of photonic crystal based structures," EPFL, Lausanne, Switzerland, Tech. Rep., 2009, doi: 10.5075/epfl-thesis-4315.

[87] Z. Ding, J. Zhou, L. Huang, F. Sun, Z. Fu, and H. Tian, "Design of side-coupled cascaded photonic crystal sensors array with ultra-high figure of merit," *Opt. Commun.*, vol. 392, pp. 68–72, Jun. 2017.

[88] Y. Xia, K. Kamata, and Y. Lu, "Photonic crystals," in *Introduction to Nanoscale Science and Technology*. Boston, MA, USA: Springer, 2004, pp. 505–529.

[89] Y.-N. Zhang, Y. Zhao, D. Wu, and Q. Wang, "Theoretical research on high sensitivity gas sensor due to slow light in slotted photonic crystal waveguide," *Sens. Actuators B, Chem.*, vol. 173, pp. 505–509, Oct. 2012.

[90] Y. Zhao, Y.-N. Zhang, and Q. Wang, "High sensitivity gas sensing method based on slow light in photonic crystal waveguide," *Sens. Actuators B, Chem.*, vol. 173, pp. 28–31, Oct. 2012.

[91] Q. Wang, Y.-N. Zhang, B. Han, and Y. Zhao, "Theory and method for enhancing sensitivity of multi-gas sensing based on slow light photonic crystal waveguide," *Optik*, vol. 125, no. 13, pp. 3172–3175, Jul. 2014.

[92] A. Kumar, T. S. Saini, and R. K. Sinha, "Design and analysis of photonic crystal biperiodic waveguide structure based optofluidic-gas sensor," *Optik*, vol. 126, no. 24, pp. 5172–5175, Dec. 2015.

[93] W.-C. Lai, W. Chakravarty, X. Wang, C. Lin, and R. T. Chen, "On-chip methane sensing by near-IR absorption signatures in a photonic crystal slot waveguide," *Opt. Lett.*, vol. 36, no. 6, pp. 984–986, Mar. 2011.

[94] Y. Chang *et al.*, "Surface-enhanced infrared absorption-based CO_2 sensor using photonic crystal slab," in *Proc. IEEE 32nd Int. Conf. Micro Electro Mech. Syst. (MEMS)*, Jan. 2019, pp. 141–144.

[95] A. Rostamian, J. Guo, S. Chakravarty, C.-J. Chung, D. Nguyen, and A. T. Chen, "Parts-per-billion carbon monoxide sensing in silicon-on-sapphire mid-infrared photonic crystal waveguides," in *Proc. Conf. Lasers Electro-Opt. (CLEO)*, May 2018, pp. 1–2.

[96] A. Afsari and M. J. Sarraf, "Design of a hydrogen sulfide gas sensor based on a photonic crystal cavity using graphene," *Superlattices Microstruct.*, vol. 138, Feb. 2020, Art. no. 106362.

[97] A. Rostamian, H. Dalir, M. H. Teimourpour, and R. T. Chen, "Sub-parts-per-million level detection of ethanol using mid-infrared photonic crystal waveguide in silicon-on-insulator," in *Conf. Lasers Electro-Opt., OSA Tech. Dig.* Optica Publishing Group, 2020, Paper STh4L.4.

[98] A. Rostamian, E. Madadi-Kandjani, H. Dalir, V. J. Sorger, and R. T. Chen, "Towards lab-on-chip ultrasensitive ethanol detection using photonic crystal waveguide operating in the mid-infrared," *Nanophotonics*, vol. 10, no. 6, pp. 1675–1682, Apr. 2021.

[99] H. Emami, M. Alidadi, A. Ebnali-Heidari, and M. Ebnali-Heidari, "Optimizing of rod-type photonic crystal waveguide methane gas sensor," *Optik*, vol. 127, no. 5, pp. 2461–2466, 2016.

[100] B. Kumari, A. Barh, R. K. Varshney, and B. P. Pal, "Silicon-on-nitride slot waveguide: A promising platform as mid-IR trace gas sensor," *Sens. Actuators B, Chem.*, vol. 236, pp. 759–764, Nov. 2016.

[101] Q. Wang, B. Han, D. Wu, and Y. Zhao, "Novel fiber optic gas sensor based on photonic crystal slow-light waveguide," *Microw. Opt. Technol. Lett.*, vol. 55, no. 8, pp. 1796–1800, Aug. 2013.

[102] Y.-N. Zhang, Y. Zhao, and Q. Wang, "Multi-component gas sensing based on slotted photonic crystal waveguide with liquid infiltration," *Sens. Actuators B, Chem.*, vol. 184, pp. 179–188, Jul. 2013.

[103] A. Zakrzewski and S. Patela, "Investigation of the laser acetylene sensor based on two-dimensional photonic crystal," *Sens. Actuators A, Phys.*, vol. 256, pp. 51–58, Apr. 2017.

[104] J. Wu, Y. Li, C. Peng, and Z. Wang, "Numerical demonstration of slow light tuning in slotted photonic crystal waveguide using microfluidic infiltration," *Opt. Commun.*, vol. 284, no. 8, pp. 2149–2152, Apr. 2011.

[105] R. Jannesari, C. Ranacher, C. Consani, T. Grille, and B. Jakoby, "Sensitivity optimization of a photonic crystal ring resonator for gas sensing applications," *Sens. Actuators A, Phys.*, vol. 264, pp. 347–351, Sep. 2017.

[106] A. Anamoradi and K. Fasihi, "A highly sensitive optofluidic-gas sensor using two dimensional photonic crystals," *Superlattices Microstruct.*, vol. 125, pp. 302–309, Jan. 2019.

[107] D. Yan, M. Meng, J. Li, and Y. Wang, "Terahertz wave refractive index sensor based on a sunflower-type photonic crystal," *Laser Phys.*, vol. 30, no. 6, Jun. 2020, Art. no. 066206.

[108] R. Ge, J. Xie, B. Yan, E. Liu, W. Tan, and J. Liu, "Refractive index sensor with high sensitivity based on circular photonic crystal," *J. Opt. Soc. Amer. A, Opt. Image Sci.*, vol. 35, no. 6, pp. 992–997, 2018.

[109] D. Nau, A. Seidel, R. B. Orzekowsky, S. H. Lee, S. Deb, and H. Giessen, "Hydrogen sensor based on metallic photonic crystal slabs," *Opt. Lett.*, vol. 35, no. 18, pp. 3150–3152, Sep. 2010.

[110] A. A. Elsayed, M. Sakr, M. Erfan, Y. M. Sabry, and D. Khalil, "On the environmental gas sensing using MEMS FTIR spectrometer in the near-infrared region," in *Proc. 33rd Nat. Radio Sci. Conf. (NRSC)*, Feb. 2016, pp. 348–355.

[111] D. Briand, O. Manzardo, N. F. de Rooij, J. Hildenbrand, and J. Wollenstein, "Gas detection using a micromachined FTIR spectrometer," in *Proc. IEEE SENSORS*, Oct. 2007, pp. 1364–1367.

[112] G. Dooly, E. Lewis, C. Fitzpatrick, and P. Chambers, "Low concentration monitoring of exhaust gases using a UV-based optical sensor," *IEEE Sensors J.*, vol. 7, no. 5, pp. 685–691, May 2007.

[113] L. Huang, H. Tian, J. Zhou, and Y. Ji, "Design low crosstalk ring-slot array structure for label-free multiplexed sensing," *Sensors*, vol. 14, no. 9, pp. 15658–15668, Aug. 2014.

[114] H. Xu, P. Wu, C. Zhu, A. Elbaz, and Z. Z. Gu, "Photonic crystal for gas sensing," *J. Mater. Chem. C*, vol. 1, no. 38, pp. 6087–6098, 2013.

[115] J. Topol'ančik, P. Bhattacharya, J. Sabarinathan, and P.-C. Yu, "Fluid detection with photonic crystal-based multichannel waveguides," *Appl. Phys. Lett.*, vol. 82, no. 8, pp. 1143–1145, 2003.

[116] T. Hasek, H. Kurt, D. S. Citrin, and M. Koch, "Photonic crystals for fluid sensing in the subterahertz range," *Appl. Phys. Lett.*, vol. 89, no. 17, Oct. 2006, Art. no. 173508.

[117] B. Wang, M. A. Dündar, R. Nötzel, F. Karouta, S. He, and R. W. Van der Heijden, "Photonic crystal slot nanobeam slow light waveguides for refractive index sensing," *Appl. Phys. Lett.*, vol. 97, no. 15, p. 151105, Oct. 2010.

[118] M. Pu, L. Liu, L. H. Frandsen, H. Ou, K. Yvind, and J. MHvam, "Silicon-on-insulator ring-shaped photonic crystal waveguides for refractive index sensing," in *Proc. Opt. Fiber Commun. Conf.*, Mar. 2010, pp. 1–3.

[119] F. Bougriou, T. Bouchemat, M. Bouchemat, and N. Paraire, "Optofluidic sensor using two-dimensional photonic crystal waveguides," *Eur. Phys. J. Appl. Phys.*, vol. 62, no. 1, p. 11201, Apr. 2013.

[120] A. Di Falco, L. O'Faolain, and T. F. Krauss, "Chemical sensing in slotted photonic crystal heterostructure cavities," *Appl. Phys. Lett.*, vol. 94, no. 6, Feb. 2009, Art. no. 063503.

[121] L. Kassa-Baghdouchea and E. Cassan, "Mid-infrared refractive index sensing using optimized slotted photonic crystal waveguides," *Photon. Nanostruct. Fundam. Appl.*, vol. 28, pp. 32–36, Feb. 2018.

[122] S. Singh, R. K. Sinha, and R. Bhattacharyya, "Photonic crystal slab waveguide-based infiltrated liquid sensors: Design and analysis," *J. Nanophotonics*, vol. 5, no. 1, Jan. 2011, Art. no. 053505.

[123] Y.-N. Zhang, Y. Zhao, Q. Wang, and K. Xue, "Liquid refractive index sensor based on slow light in slotted photonic crystal waveguide," *Optik*, vol. 124, no. 22, pp. 5443–5446, Nov. 2013.
[124] F. Bougriou, T. Boumaza, M. Bouchemat, and N. Paraire, "Sensitivity analysis of a photonic crystal waveguide for refraction index sensing," *Phys. Scripta*, vol. T151, Nov. 2012, Art. no. 014064.
[125] M. Turduev *et al.*, "Mid-infrared T-shaped photonic crystal waveguide for optical refractive index sensing," *Sensors Actuators B, Chem.*, vol. 245, pp. 765–773, Jun. 2017.
[126] J. Witzens, M. Hochberg, T. Baehr-Jones, and A. Scherer, "Mode matching interface for efficient coupling of light into planar photonic crystals," *Phys. Rev. E, Stat. Phys. Plasmas Fluids Relat. Interdiscip. Top.*, vol. 69, no. 4, Apr. 2004, Art. no. 046609.
[127] H. S. Dutta, A. K. Goyal, V. Srivastava, and S. Pal, "Coupling light in photonic crystal waveguides: A review," *Photon. Nanostruct. Fundamentals Appl.*, vol. 20, pp. 41–58, Jul. 2016.
[128] Q. Zhao, K. Cui, X. Feng, F. Liu, W. Zhang, and Y. Huang, "Low loss sharp photonic crystal waveguide bends," *Opt. Commun.*, vol. 355, pp. 209–212, Nov. 2015.
[129] X. Zhao, Y. Li, S. Feng, X. Chen, C. Li, and Y. Wang, "Beam splitting characteristics of two-dimensional photonic crystals based on surface modulation," *Opt. Commun.*, vol. 439, pp. 193–200, May 2019.
[130] L. Wu, M. Mazilu, T. Karle, and T. F. Krauss, "Superprism phenomena in planar photonic crystals," *IEEE J. Quantum Electron.*, vol. 38, no. 7, pp. 915–918, Jul. 2002.
[131] D. N. Chigrin, A. V. Lavrinenko, D. A. Yarotsky, and S. V. Gaponenko, "Observation of total omnidirectional reflection from a one-dimensional dielectric lattice," 1998, *arXiv:cond-mat/9811073*.
[132] Y. Fink *et al.*, "A dielectric omnidirectional reflector," *Science*, vol. 282, no. 5394, pp. 1679–1682, 1998.
[133] P. S. J. Russell, S. Tredwell, and P. J. Roberts, "Full photonic bandgaps and spontaneous emission control in 1D multilayer dielectric structures," *Opt. Commun.*, vol. 160, nos. 1–3, pp. 66–71, Feb. 1999.
[134] V. A. Tolmachev, T. S. Perova, J. Ruttle, and E. V. Khokhlova, "Design of one-dimensional photonic crystals using combination of band diagram and photonic gap map approaches," *J. Appl. Phys.*, vol. 104, no. 3, Aug. 2008, Art. no. 033536.
[135] A. Bouzidi, D. Bria, A. Akjouj, Y. Pennec, and B. Djafari-Rouhani, "A tiny gas-sensor system based on 1D photonic crystal," *J. Phys. D, Appl. Phys.*, vol. 48, Nov. 2015, Art. no. 495102.
[136] H. Clevenson, P. Desjardins, X. Gan, and D. Englund, "High sensitivity gas sensor based on high-Q suspended polymer photonic crystal nanocavity," *Appl. Phys. Lett.*, vol. 104, no. 24, Jun. 2014, Art. no. 241108.
[137] Z. A. Zaky, A. M. Ahmed, A. S. Shalaby, and A. H. Aly, "Refractive index gas sensor based on the Tamm state in a one-dimensional photonic crystal: Theoretical optimisation," *Sci. Rep.*, vol. 10, no. 1, pp. 1–9, Dec. 2020.
[138] S. Y. Lin *et al.*, "A three-dimensional photonic crystal operating at infrared wavelengths," *Nature*, vol. 394, no. 6690, pp. 251–253, Jul. 1998.
[139] S. Takahashi *et al.*, "Direct creation of three-dimensional photonic crystals by a top-down approach," *Nature Mater.*, vol. 8, no. 9, pp. 721–725, Sep. 2009.
[140] S. Ogawa, M. Imada, S. Yoshimoto, M. Okano, and S. Noda, "Control of light emission by 3D photonic crystals," *Science*, vol. 305, no. 5681, pp. 227–229, Jul. 2004.
[141] S. Maruo, O. Nakamura, and S. Kawata, "Three-dimensional microfabrication with two-photon-absorbed photopolymerization," *Opt. Lett.*, vol. 22, no. 2, pp. 132–134, 1997.
[142] K.-S. Lee, D.-Y. Yang, S. H. Park, and R. H. Kim, "Recent developments in the use of two-photon polymerization in precise 2D and 3D microfabrications," *Polym. Adv. Technol.*, vol. 17, no. 2, pp. 72–82, 2006.
[143] Y. Li *et al.*, "High-contrast infrared polymer photonic crystals fabricated by direct laser writing," *Opt. Lett.*, vol. 43, no. 19, pp. 4711–4714, 2018.
[144] J. Serbin, A. Ovsianikov, and B. Chichkov, "Fabrication of woodpile structures by two-photon polymerization and investigation of their optical properties," *Opt. Exp.*, vol. 12, no. 21, pp. 5221–5228, 2004.

Anuj Singhal (Graduate Student Member, IEEE) received the Bachelor of Technology degree in electronics and communication engineering from Kurukshetra University, Thanesar, India, in 2017. He is pursuing the Ph.D. degree with the Micromechatronics Systems Laboratory, University of Illinois at Chicago, Chicago. His thesis focuses on the development of novel sensor assemblies based on photonic crystals for gas detection at single-digit ppm levels.

He then moved to Chicago, IL, USA, in 2017. He also works as a Research Assistant with the Nanotechnology Core Facility (NCF), where he supervises micro electro mechanical systems (MEMS)/nano electro mechanical systems (NEMS) fabrication processes.

Igor Paprotny (Member, IEEE) received the Ph.D. degree in Computer Science from Dartmouth College, Hanover, NH, USA.

He is currently an Associate Professor with the Department of Electrical and Computer Engineering, University of Illinois at Chicago, Chicago, IL, USA. He is also the Consortium Lead for the Air-Microfluidics Group (AMFG). He has authored five book chapters, over 50 papers in journals and conferences, and holds four patents. His research interests include microrobotics, energy systems sensing, and air-microfluidics.